H. R. Ziaei Moghadam¹, S. A. Faghidian¹, M. Jamal-Omidi²*, S. Rahmati¹

Micro-Residual Stress Measurement in Nanocomposite Reinforced Polymers

In the present study, residual stress is measured in fiber-reinforced SWCNT/epoxy at weight fractions of 0.1% and 0.5% with a cross-ply layup on a micro-scale. The mechanical properties of the SWCNT/epoxy composites were determined by tensile testing and the Young's modulus of the epoxy increased moderately with the addition of CNTs. The micro-residual stress of the cross-ply CF/epoxy and CNF-reinforced CF/epoxy laminates were measured using a new experimental approach. The micro-hole was milled by laser beam and the surface displacement was recorded by SEM after milling. In order to determine the residual stress from the recorded strain, the calibration matrix was calculated using the finite element method. The residual stress was obtained at a certain hole depth of specimens. The reliability of this approach was assessed by comparing the residual stress measurements from this method and from the standard hole-drilling method. The experimental results of the present approach confirmed that laser hole drilling SEM-DIC has excellent potential as a reliable method for measuring residual stress in polymer nanocomposites. Generally, CNT agglomerates, especially in high weight fractions, increased the micro-residual stress. An analytical method based on classical theory was used to calculate the residual stress and was compared with the experimental results. Good agreement was found between the results of the analytical methods and the experimental measurement.

1 Introduction

Residual stresses can occur in many types of materials during the manufacturing process and cause undesirable mechanical performance. In some situations, residual stresses may play an effective role in applications such as inelastic beam bending, laser-forming and shot peening (Faghidian, 2014). Curing at a relatively high processing temperature and the subsequent cooling to room temperature can increase residual stress in polymer composites due to the significant differences in shrinkage between the matrix and the fibers. Residual stress

can cause matrix cracking, delamination, changes in the material properties and warpage (Xi et al., 2018; Hamidi and Altan, 2017; Jones et al., 2017). Therefore, it is important to appropriately measure and reconstruct the residual stress in reinforced polymers (Faghidian, 2013; 2014; 2015a; 2015b; 2017).

The methods used to measure residual stress can be divided into non-destructive and destructive categories. In non-destructive methods such as x-ray diffraction (Allain et al., 2018; Zhou et al., 2017; Lin et al., 2017), magnetics (Ding et al., 2018; Lasaosa et al., 2018), neutron diffraction (Jimenez-Mena et al., 2019; Ahn et al., 2018; Jiang et al., 2018) and the Raman method (Kollins et al., 2018; Jana et al., 2017), it is not necessary to remove a piece of the sample. However, destructive methods such as hole-drilling (Nobre et al., 2018; Smit and Reid, 2018; Peral et al., 2017), ring-coring (Ghaedamini et al., 2018; Giri and Mahapatra, 2017) or the slitting method (Jones and Bush, 2017) require the removal of a piece of the material for testing. All of these experimental methods are usually employed to measure residual stress at a macro-scale. The measurement of residual stress on the micro-scale is similar to the destructive methods which include the removal of a piece of material. However, the dimensions of the removed material, such as a slit or hole, are on the micro-scale. Consequently, the relieved displacement field is micro-scale. This micro-measurement approach is employed in micro-slitting (Zhang, 2018; Xu and Bao, 2017), micro-ring-coring (Pan et al., 2019; Korsunsky et al., 2018; Salvati and Korsunsky, 2017) and holedrilling (Salvati et al., 2016).

The displacement caused by removal on the macro-scale can be effectively measured by a strain-gauge rosette. However, strain gauges lack sufficient precision on the micro-scale; thus, experimental measurement methods such as SEM-DIC should be employed. In the SEM-DIC method, scanning electron microscopy (SEM) can produce images with excellent resolution before and after micro-milling. Afterward, digital image correlation (DIC) can be used to compare images and determine displacement caused by the relieved residual stresses in specific directions. In SEM-DIC residual stress measurement, focused ion beam (FIB) machining is usually used for removal of material for milling at the nano-scale (Pan et al., 2019; Korsunsky et al., 2018; Salvati and Korsunsky, 2017; Salvati et al., 2016).

In fiber-reinforced polymer composites, a macro-residual stress is generally produced by the different mechanical properties of each layer during the curing and cooling stages of fabrication. Also, residual stress at the micro-scale can be caused

¹Department of Mechanical Engineering, Science and Research Branch, Islamic Azad University, Tehran, Iran

²Department of Aerospace Engineering, Space Research Institute, Malek-Ashtar University of Technology, Tehran, Iran

^{*} Mail address: Majid Jamal-Omid, Department of Aerospace Engineering, Space Research Institute, Malek-Ashtar University of Technology, Tehran, 15875-1774, Iran E-mail: j_omidi@mut.ac.ir; m.jamalomidi@gmail.com

by a mismatch in the coefficient of thermal expansion (CTE) between the fibers and the matrix (Jain et al., 2017). Procedures for preventing residual stress in fiber-reinforced polymer composites include changes in curing or layer arrangement (Shah et al., 2018). However, adding nanoparticles to a fiber-reinforced polymer (FRP) is a novel and more consistent method of reducing the residual stress and improving dimensional stability. A high Young's modulus and negative thermal expansion carbon nanotubes (CNTs) or nanofibers make them suitable candidates for minimizing the differences between the Young's modulus and CTE of the fiber and matrix, decreasing the residual stress in FRPs (Shokrieh et al., 2013). However, the effects of CNTs or carbon nanofibers (CNFs) on the residual stress should be investigated in the micro-scale (Ghasemi et al., 2017; Rahimian-Koloor et al., 2018; Shokrieh et al., 2014).

In the present study, the effects of CNTs on micro-residual stress in carbon fiber (CF)/epoxy composites are experimentally examined. Laser beam machining (LBM) was employed for milling and removal of material by forming micro-holes. The SEM-DIC method was then utilized to determine the micro-displacement caused by the relieved residual stress. To the best of the authors' knowledge, no study has used this method to measure residual stress on a micro-scale. To investigate the effects of CNTs on micro-residual stress, 0.1% and 0.5% CNTs were used in the CF/epoxy composite. The coefficient matrix to transform the released strain to residual stress is calculated using finite element (FE) analysis and the mechanical properties of the material were experimentally measured.

2 Experimental Procedure

In the present study, two phases CF/epoxy composites and three phases CNT/CF/epoxy composites were fabricated. The CNTs were dispersed in the composites at weight fractions of 0.1% and 0.5%. A new hole-drilling method was used to measure the micro-residual stress using a laser beam machine for drilling and SEM-DIC to determine the relieved strain after hole-drilling. For residual stress measurement, the dimensions of the samples were 15×15 mm with a 1-mm thickness. Epon epoxy resin 828 (Hexion, Columbus, USA) and unidirectional T300 CFs (Toray, Tokyo, Japan) were used to fabricate the cross–ply laminate with a $[0_2/90_2]_s$ layup. To confirm the accuracy of the proposed method, laser SEM-DIC was first applied to nanocomposites having different weight fractions and the dispersion quality and experimentally measured residual stress were compared to the measurements available in the literature.

In order to fabricate highly agglomerated nanocomposites, epoxy resin 828 was first mixed with the CNT, stirred with a mechanical stirrer for 30 min at 2000 min⁻¹ with a stirrer and placed under vacuum to remove air bubbles. During stirring, the mixture was placed in an ice bath and three phases CNT/CF/epoxy laminate were fabricated using the handy lay-up method. The fabricated laminates were cast into steel molds and cured at 100 °C for 6 h and then allowed to gradually cool at room temperature. The slightly agglomerated nanocomposites were fabricated similarly to the highly agglomerated nanocomposites, except for sonication at 200 W with a probe of 14 mm after stirring. For the CNT fractions of 0.1% and 0.5%, sonication times of 40 and 60 min were used, respec-

tively. Once sonication was complete, the curing agent was added and stirred for 20 min at 250 min⁻¹. The mixture was then placed in a vacuum chamber for 30 min to completely remove the air bubbles.

The mechanical characteristics of the composite samples are determined using testing standards. The Young's moduli of E_x and E_y in the longitudinal and transverse directions and tensile testing on two- and three-phases composites were performed according to ASTM D3039 (2017). The dimensions of the unidirectional samples were $250\times15~\text{mm}$ with a thickness of 1.2 mm and $175\times25~\text{mm}$ with a thickness of 2 mm at 0° and 90° layers, respectively, as shown in Fig. 1. For each tensile test on the composite specimens with different CNT contents, at least three samples were tested and characterized.

3 Residual Stress Measurement

Several methods exist in the literature to measure residual stress in materials, which fall into destructive and non-destructive categories. Hole-drilling is an applicable method that is generally used for residual stress measurement according to ASTM 837 (2013). In ASTM 837 (2013), strain gauges should be used to measure the relieved strain after hole drilling that is generally caused by macro-residual stress. However, strain gauges are not sufficiently accurate to measure residual stress on the micro-scale. Therefore, a new approach, the SEM-DIC method, has been employed here to determine the micro-residual stress in the nanocomposite reinforced polymers. The hole was created with a laser beam having a diameter of 180 μm and the SEM-DIC method was used to determine the relieved strain in all directions. To this end, the micro-polyester was used as a decoration to find a regular pattern of digital image correlation.

3.1 Laser SEM-DIC Method

The common methods for measuring residual stress can be also used for residual stress on the micro-scale by reducing the scales for smaller samples. The constraint for reducing the scale in the hole-drilling method is the hole diameter created by traditional drilling methods. The traditional method also affects the released residual stress. Because of the CF content of polymer composites, traditional methods of applying tensile stress to remove the CF connections affect the residual stress distribution confined in the composite caused by the direction of the layers. These restrictions can be effectively removed with the use of laser beam drilling, which creates a hole using a laser beam under shear stress. A 100 µm hole diameter can



Fig. 1. Unidirectional samples for tensile tests in longitudinal and transverse direction

be created using laser drilling at a time duration needed to create a hole in polymer composites of less than 0.1 s.

This drilling process, when applied onto nanocomposite-reinforced polymers, can merely remove the CF without introducing tensile stress. Another restriction to residual stress measurement on the micro-scale is the use of a rosette strain gauge for measurement of the released displacement after hole-drilling. The accuracy of commercial strain gauges is not sufficient for detection of the micro-displacement released after formation of the micro-holes. The displacement released after hole drilling can be determined with high accuracy utilizing SEM to capture images before and after micro-hole drilling at high resolution. The pixel intensity is normally assumed to remain constant. The purpose of the DIC method is to produce displacement and strain fields within a region of interest (ROI) for a sample undergoing deformation. This is performed by dividing the reference image into small subsections called subsets and determining their respective locations in the current image. The mathematical details of the DIC method can be found in Baker and Matthews (2004), Pan et al. (2009) and Blaber et al. (2015).

3.2 Obtaining Full Field Strains

Strains are harder to obtain than the displacement field, because the strain field contains differentiation, which is noise sensitive. Consequently, any noise in the displacement field could cause multiple errors in the strain field. The Green-Lagrangian strain can be determined as:

$$E_{xx} = \frac{1}{2} \left(2 \frac{\partial u}{\partial x} + \left(\frac{\partial u}{\partial x} \right)^2 + \left(\frac{\partial v}{\partial x} \right)^2 \right), \tag{1}$$

$$E_{xy} = \frac{1}{2} \left(\frac{\partial u}{\partial y} + \frac{\partial v}{\partial x} + \frac{\partial u \partial u}{\partial x \partial y} + \frac{\partial v \partial v}{\partial x \partial y} \right), \tag{2}$$

$$E_{yy} = \frac{1}{2} \left(2 \frac{\partial v}{\partial y} + \left(\frac{\partial u}{\partial y} \right)^2 + \left(\frac{\partial v}{\partial y} \right)^2 \right), \tag{3}$$

where E_{xx} , E_{yy} and E_{xy} are strain fields in the x and y directions and the shear strain in the xy plane, respectively. The displacement gradients can be directly determined through the inverse compositional Gauss-Newton (ICGN) (Baker and Matthews, 2004) scheme. However, the displacement gradients are noisy; thus, they should be flattened before obtaining the strain fields.

After it is applied to the entire displacement field, the strain field is calculated. In order to verify the proposed method, the residual stress is measured using the standard hole-drilling method according to ASTM E-837 (2013). For each CNT weight fraction and dispersion method, at least five samples were tested and the final strain was considered to be the average result of the five tests. These samples have been tested using the SEM-DIC method. SEM images of the samples before and after hole-drilling using the DIC algorithm and the strain determined through the present method were compared with those obtained using the standard hole-drilling method.

4 Finite Element Modeling

After determining the strain using the SEM-DIC method, the residual stress can be calculated. For the hole-drilling measurement method, the residual stress distribution was assumed to have plane stress status. Several models are available to measure relieved strain to residual stress for both isotropic and orthotropic materials (Faghidian, 2016). In the traditional residual stress measurement, the relieved strain in the direction of the strain gauges is related to the residual stress components as (Bert and Thompson, 1968):

$$\varepsilon_{\rm r} = A(\sigma_{\rm x} + \sigma_{\rm y}) + B(\sigma_{\rm x} - \sigma_{\rm y})\cos 2\theta + C\tau_{\rm xy}\sin 2\theta,$$
 (4)

where θ is the angle of the strain gauge direction with respect to the x-axis, and A, B and C are the calibration factors. Furthermore, σ_x , σ_y and τ_{xy} are the in-plane components of the residual stress. The calibration factors in Eq. 4 depend on the material properties, hole-depth and stress measurement location.

For orthotropic material behavior, the components of the residual stress field can be shown to be related to measured strains ε_1 , ε_2 and ε_3 through a generalized matrix form of (Schajer and Yang, 1994):

$$\frac{1}{\sqrt{E_x E_y}} \begin{bmatrix} C_{11} & C_{12} & C_{13} \\ C_{21} & C_{22} & C_{23} \\ C_{31} & C_{32} & C_{33} \end{bmatrix} \begin{bmatrix} \sigma_x \\ \tau_{xy} \\ \sigma_y \end{bmatrix} = \begin{bmatrix} \epsilon_1 \\ \epsilon_2 \\ \epsilon_3 \end{bmatrix}, \tag{5}$$

where $1/\sqrt{E_x E_y}$ is used to make dimensionless the coefficient factors. The calibration matrix elements can be generally carried out numerically or experimentally. In the present study, the calibration coefficients are determined by finite element (FE) simulation using the material constants obtained by experimental measurements. The geometry of the samples along with the dimension of the hole were simulated in the ABAQUS FE software (2016), Dassault Systemes, Vélizy-Villacoublay, France. A continuous 8-noded linear brick 3D element was utilized and an FE mesh was used in the vicinity of the hole at 20 % of the hole diameter as shown in Fig. 3.

The hole drilling was modeled by removing the elements from the hole location. Simple tensile stress with unit load were applied in the fiber direction where strain gauges 1, 2 and 3 are located. The strain released after hole-drilling was determined and used to calibrate the coefficient matrix.

In order to transform each load in the direction of the polar coordinates, the following stress transformation equation is used:

$$\begin{split} &\sigma_{rr} = \sigma_x \cos^2 \theta + \sigma_y \sin^2 \theta + \tau_{xy} \sin 2\theta, \\ &\tau_{r\theta} = -\frac{\sigma_x - \sigma_y}{2} \sin 2\theta + \sigma_y \sin^2 \theta + \tau_{xy} \cos 2\theta. \end{split} \tag{6}$$

Separate application of the unit load for each direction on the strain gauge and calculation of the polar components of the stress is done as follows:

$$\begin{split} &\sigma_x = 1, \sigma_y = \tau_{xy} = 0, \sigma_{rr} = \cos^2\theta, \tau_{r\theta} = -\frac{\sin 2\theta}{2}, \\ &\sigma_y = 1, \sigma_x = \tau_{xy} = 0, \sigma_{rr} = \sin^2\theta, \tau_{r\theta} = \frac{\sin 2\theta}{2}, \\ &\tau_{xy} = 1, \sigma_x = \sigma_y = 0, \sigma_{rr} = \sin 2\theta, \tau_{r\theta} = \cos 2\theta. \end{split} \tag{7}$$

The calibration factors can be obtained using Eq. 5 by knowing the stress and resulting strain values. The calibration factors depend on the material properties, sample geometry, hole depth and strain gauge positions.

5 Analytical Analysis

In order to ensure the reliability of the results of the proposed experimental method, the analytical solution was used to determine the micro-residual stress caused by the differences in the curing and ambient temperatures and the results were compared with the experimental results. Classical lamination theory was used to determine the analytical solution. Calculation of the residual stress using classical lamination theory requires information about the thickness, mechanical and thermal properties of the composite material. As mentioned, the mechanical properties were determined using the standard test (ASTM D3039, 2017). Information about each material from the manufacturers was used to fabricate the composites. The coefficient of thermal expansion (CTE) of the composite material was calculated using the modified Scharpery relation that assumes that the CNTs are well dispersed in the matrix in random directions as (Alamusi et al., 2013):

$$\begin{split} \alpha_c &= \frac{1}{2} \left[\frac{V_{NT} E_{NT} \alpha_{NT} + V_m E_m \alpha_m}{V_{NT} E_{NT} + V_m E_m} (1 - \upsilon_{NT} V_{NT} - \upsilon_m V_m) \right. \\ &+ \left. (1 + \upsilon_m) \alpha_m V_m + (1 + \upsilon_{NT}) \alpha_{NT} V_{NT} \right], \end{split} \tag{8}$$

where E, V and α are the modulus of elasticity, weight fraction and CTE, respectively, and NT and m are the CNT and matrix, respectively. Because the good dispersion of the CNTs is assumed, the results of the analytical method can be compared with the results of the experimentally measured residual stress of well-dispersed samples.

Because of the orthotropic properties of each composite layer, the longitudinal and transverse CTE of each layer should be determined. The longitudinal CTE is calculated as follows (Schapery, 1968):

$$\alpha_1 = \frac{E_f \alpha_f V_f + E_m \alpha_m V_m}{E_f V_f + V_m E_m} = \frac{\left(E\alpha\right)_1}{E_1}. \tag{9}$$

The transverse CTE is determined as follows (Hashin, 1979):

$$\begin{split} \alpha_2 &= \alpha_{2f} V_f \bigg(1 + \upsilon_{12f} \frac{\alpha_{1f}}{\alpha_{2f}} \bigg) + \alpha_{2m} V_m \bigg(1 + \upsilon_{12m} \frac{\alpha_{1m}}{\alpha_{2m}} \bigg) \\ &- \big(\upsilon_{12f} V_f + \upsilon_{12m} V_m \big) \frac{(E\alpha)_1}{E_1}. \end{split} \tag{10}$$

Knowing the CTE of each ply, for the orthotropic layer, the offaxis direction CTE can be calculated as follows:

$$\begin{split} \{\alpha\}_{off}^{(k)} &= \left\{ \begin{matrix} \alpha_1 \\ \alpha_2 \\ \alpha_3 \end{matrix} \right\}^k = \left[\begin{matrix} m^2 & n^2 & -mn \\ n^2 & m^2 & mn \\ 2mn & -2mn & m^2 - n^2 \end{matrix} \right]^k \left\{ \begin{matrix} \alpha_x \\ \alpha_y \\ 0 \end{matrix} \right\}, \\ m &= cos(\theta), \ n = sin(\theta), \end{split}$$

where θ is the orientation of each ply rather than the mid-plane and α_x , α_y and α_1 , α_2 , α_3 are the CTE values in the on- and off-axis directions, respectively, and k is the number of plies.

The thermal load and moments in the off-axis direction for the laminated composite can be calculated as follows:

$$\left(N_{1}^{T},M_{1}^{T}\right)=\sum_{k=1}^{n}\bigl(\bar{Q}_{11}^{k}\alpha_{1}^{k}+\bar{Q}_{12}^{k}\alpha_{2}^{k}+\bar{Q}_{16}^{k}\alpha_{6}^{k}\bigr)\Delta T(t_{k},t_{k}z_{k}),$$

$$(N_2^T, M_2^T) = \sum_{k=1}^n (\bar{Q}_{21}^k \alpha_1^k + \bar{Q}_{22}^k \alpha_2^k + \bar{Q}_{26}^k \alpha_6^k) \Delta T(t_k, t_k z_k),$$
 (12)

$$\left(N_{6}^{T}, M_{6}^{T}\right) = \sum_{k=1}^{n} \bigl(\bar{Q}_{61}^{k} \alpha_{1}^{k} + \bar{Q}_{62}^{k} \alpha_{2}^{k} + \bar{Q}_{66}^{k} \alpha_{6}^{k}\bigr) \Delta T(t_{k}, t_{k} z_{k}),$$

where t_k , z_k and $\Delta T^{(k)}$ are the thickness of each layer, distance of each layer to the laminate mid-plane and temperature difference between the cure and ambient conditions, respectively, and $\alpha_i^{(k)}$ and $\left[\bar{Q}_{ij}\right]^{(k)}$ are the CTE and stiffness matrix. After calculating the thermal loads and moments using

After calculating the thermal loads and moments using Eq. 12, the strain and curvature of the mid-plane of the laminate can be determined as follows:

$$\begin{cases}
\epsilon^{\circ} \\
\kappa^{\circ}
\end{cases} = \begin{bmatrix}
A & B \\
A & D
\end{bmatrix} \begin{Bmatrix}
N^{T} \\
M^{T}
\end{Bmatrix},$$
(13)

where A, B, and D are the in-plane laminate moduli, in-plane/ flexure laminate coupling moduli and flexural laminate stiffness matrices, respectively. After calculating ϵ° and κ° using Eq. 13, the residual stress of each ply in the off-axis coordinate system can be obtained as follows:

$$\{\sigma_{rs}\}_{off}^{(k)} = \left[\bar{Q}_{ij}\right]^{(k)} \Big(\{\epsilon^{\circ}\} + z_k\{\kappa^{\circ}\} - \{\alpha\}_{off}^{(k)}\Delta T\Big). \tag{14} \label{eq:tau_state}$$

The residual stress calculated above was compared with the experimental stress determined using the DEM-DIC method.

6 Results and Discussion

The average results of tensile testing for all CF-CNT/epoxy composites in the longitudinal and transverse directions are shown in Table 1 for poor dispersed and well-dispersed composites. Table 1 shows that the modulus of elasticity of the nanocomposites increased as the weight fraction of the CNTs increased in comparison with composites without CNTs, regardless of the CNT agglomeration. This is in agreement with the results reported in the literature (Ziaei Moghadam et al., 2019). However CNT agglomerations directly affected the modulus of elasticity of the nanocomposites. For nanocomposites with a 0.1 % CNT weight fraction, the modulus of elasticity of the well-dispersed sample showed a mild increase in comparison with the poorly dispersed samples. For nanocomposites with a 0.5 % CNT weight fraction, agglomeration inversely affected the modulus of elasticity of the nanocomposite. As observed in Table 1, the modulus of elasticity of the well-dispersed sample was lower than for the poorly dispersed samples. Similar results have been reported in previous research (Song and Youn, 2005). This result is similar to the poorly dispersed samples, where CNT agglomeration fills the spaces between the CNTs and nanocomposites. This changes the behavior of the nanocomposites to that of a material with a lower weight fraction. After tensile testing of the CNT/epoxy

composites, field emission electron microscopy (FESEM) images of the fracture surface are shown in Fig. 2. The FESEM image clearly demonstrates that the CNTs dispersed in the polymer without sonication have formed agglomerates. As shown in Fig. 2A for the sonicated samples, slight agglomeration of the CNTs can be observed. Figure 2B shows the increased weight of the CNT agglomerates on the surface of the nanocomposites.

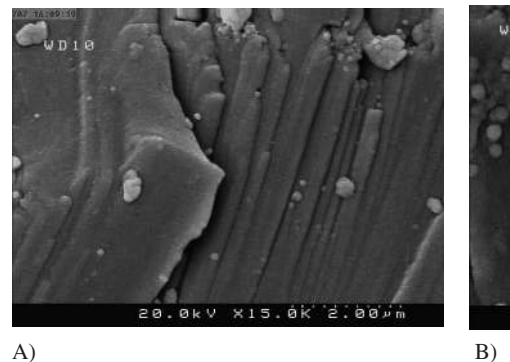
The elastic moduli of the samples in Table 1 were used in ABAQUS FE software to introduce the material properties. In order to determine the elements of calibration matrixes C_{11} , C_{21} and C_{31} , a unit load was applied in the x-direction and in the y-direction to obtain C_{13} , C_{23} and C_{33} . For remaining calibration elements C_{12} , C_{22} and C_{32} , a shear unit load was applied and, as expected, $C_{12} = C_{32} = 0$ was obtained (Schajer and

Yang, 1994). The calibration coefficient as determined by the FE method is shown in Table 2. The FE simulation model of hole-drilling is presented in Fig. 3.

The thickness of each layer of samples and the depth of the hole created by laser was determined by optical microscopy. Prior to measuring the relieved strain due to the micro-hole and calculating the residual stress, the reliability of the proposed method was assessed by comparing the relieved strain at the macro-level using the standard hole drilling method according to ASTM 837 (2013) and the present method. The same dimensions, hole diameter, hole depth, strain gauge dimension and positions were used in all samples for comparison. Table 3 shows the results of the measured strains in the 0° layer by both methods and $\Delta\epsilon\%$ represents the relative error in each sample. Tables 4 and 5 compare the measured strain

CNTs wt.%	0	0.1% poor-dispersed	0.1% well-dispersed	0.5% poor-dispersed	0.5% well-dispersed
Modulus	E	E	E	E	E
	(GPa)	(GPa)	(GPa)	(GPa)	(GPa)
Longitudinal	42.93	45.59	47.61	53.60	49.14
	[1.55]	[2.95]	[1.31]	[1.81]	[3.39]
Transverse	2.27	2.33	2.6	3.53	3.12
	[2.20]	[3.39]	[2.35]	[3.27]	[2.33]

Table 1. Young's modulus of polymer composite after addition of CNT for different qualities of dispersion (standard deviation in brackets)



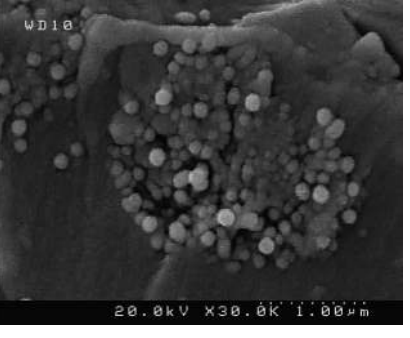


Fig. 2. FESEM images of CNT/CF/epoxy nanocomposites, formation of agglomerates: A) sonicated sample with less agglomeration, B) sample without sonication and increased agglomeration

0.1 % poor-dispersed	0.1 % well-dispersed				
$\begin{bmatrix} -12.313 & 0 & 6.93 \\ -7.094 & 73.359 & -28.489 \\ 12.96 & 0 & -79.774 \end{bmatrix}$	$\begin{bmatrix} -11.765 & 0 & 6.544 \\ -2.35 & 66.584 & -25.371 \\ 11.777 & 0 & -71.687 \end{bmatrix}$				
0.5 % poor-dispersed	0.5 % well-dispersed				
$\begin{bmatrix} -10.097 & 0 & 5.563 \\ -2.066 & 51.119 & -18.459 \\ 9.512 & 0 & -53.540 \end{bmatrix}$	$\begin{bmatrix} -11.099 & 0 & 6.128 \\ -2.256 & 57.439 & -21.026 \\ 10.564 & 0 & -60.569 \end{bmatrix}$				

Table 2. Calibration coefficient calculated using FE method

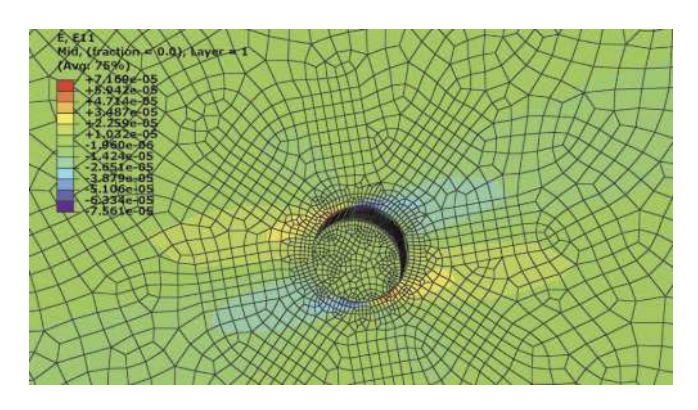


Fig. 3. FE simulation model of hole-drilling

using the standard method and laser SEM-DIC method in the 135° and 270° directions, respectively. In the laser SEM-DIC method, image magnification in SEM was $40\times$, DIC analysis used 43×43 pixel patches with 12-pixel spacing and the laser beam exposure time was 0.1 s.

The measurement results presented in Tables 3, 4 and 5 show that the proposed methods of laser hole drilling and SEM-DIC had acceptable error in comparison with the traditional hole-drilling method. Measurement of the released strain shows that a higher weight fraction of CNTs in the nanocomposite decreased the released strain. Moreover, for the 0.1% and 0.5% CNT weight fractions, well-dispersed samples released smaller amounts of strain in comparison with poorly dispersed samples. This difference was greater for nanocomposites with the 0.5%

Extraction strains	CNTs wt.%							
	0	0.1 % poor- dispersed	0.1 % well- dispersed	0.5 % poor- dispersed	0.5 % well- dispersed			
From hole drilling method	55 [5.14]	49 [6.43]	46 [4.37]	45 [7.11]	40 [3.29]			
From laser SEM-DIC method	60 [4.21]	45 [6.54]	50 [2.94]	41 [8.62]	35 [2.46]			
Error Δε%	9.09	8.16	8.69	8.88	12.5			

Table 3. Average value of experimentally measured strains (µE) in 0° gauge direction (standard deviation in brackets)

Extraction strains	CNTs wt.%							
	0	0.1 % poor- dispersed	0.1 % well- dispersed	0.5 % poor- dispersed	0.5 % well- dispersed			
From hole drilling method	-79 [6.32]	-69 [7.35]	-63 [5.24]	-61 [9.21]	-34 [5.67]			
From Laser SEM-DIC method	-88 [7.66]	-70 [5.34]	–67 [4.52]	-55 [6.92]	-29 [3.36]			
Error $\Delta \epsilon \%$	11.39	1.42	6.35	9.83	14.7			

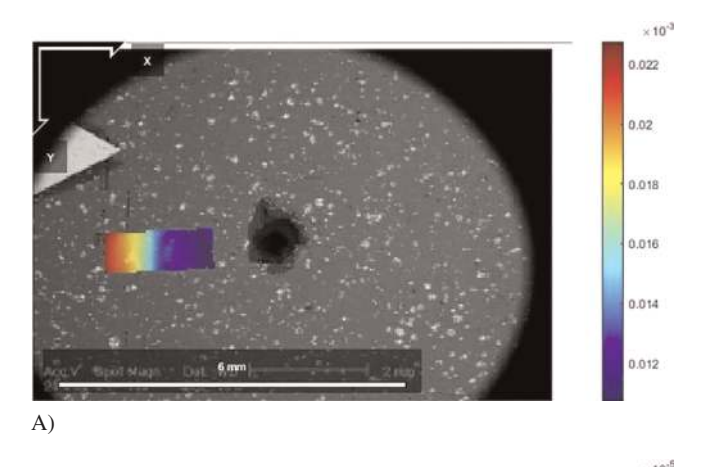
Table 4. Average value of experimentally measured strains (µE) in 135° gauge direction (standard deviation in brackets)

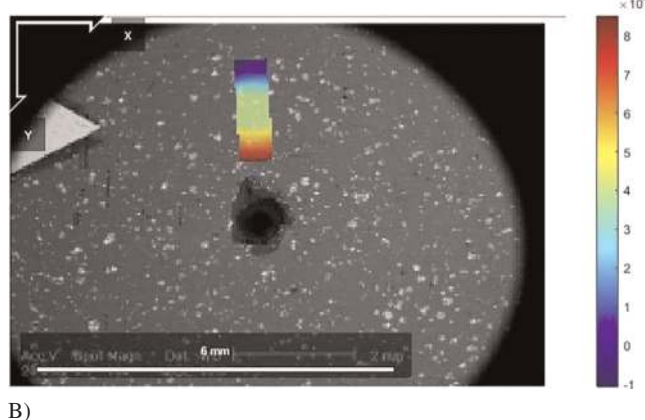
Extraction strains	CNTs wt.%						
	0	0.1 % poor- dispersed	0.1 % well- dispersed	0.5 % poor- dispersed	0.5 % well- dispersed		
From hole drilling method	-240 [13.14]	-201 [10.68]	-199 [9.53]	-210 [11.27]	-170 [10.32]		
From Laser SEM-DIC method	-265 [15.20]	-189 [12.54]	-211 [13.49]	-229 [16.31]	-158 [12.74]		
Error $\Delta \epsilon \%$	10.42	5.97	6.03	9.04	7.05		

Table 5. Average value of experimentally measured strains ($\mu\epsilon$) in 270° gauge direction (standard deviation in brackets)

CNT weight fraction. A maximum error of 14.7% was observed for strains in the 135° direction. This demonstrates the acceptable accuracy of the method used in this study. In order to measure the relieved micro-strain, a hole with a diameter of $180~\mu m$ and depth of 0.375~mm was created using a laser beam. Figure 4 shows the analysis using the DIC method on SEM images in the 0° , 90° and 45° directions.

The strains shown in Table 6 result from processing the SEM images before and after micro-drilling using a DIC algorithm. As shown in Table 6, the addition of CNTs to the poly-





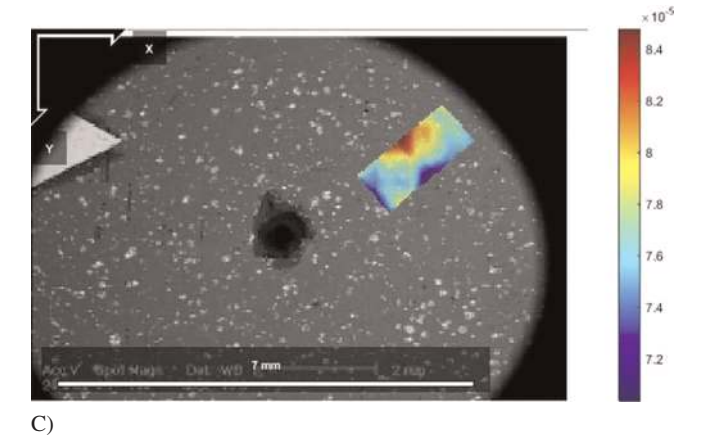


Fig. 4. Strain distribution obtained by SEM-DIC method after formation of micro-hole at A) 0° , B) 90° , C) 45°

mer matrix will generally decrease the measured micro-strain in all directions. However, a higher weight fraction and poor dispersion of CNTs made an exception, because of the CNT agglomeration that formed due to poor dispersion resulted in stress concentration, neutralizing the effect of the CNTs. CNT agglomeration caused higher strain than the sample without CNTs and a significant decrease in strain can be observed in the well-dispersed CNTs. Therefore, the parameters of higher weight fraction and good dispersion of CNTs play a vital role in reducing the relieved micro-strain.

Micro-residual stress can be subsequently determined using the measured micro-strain as shown in Table 6 and the calibration coefficient matrix in Eq. 5. The variation in the determined micro-residual stress for each sample is shown in Tables 7 and 8 for the x- and y-directions, respectively. Due to symmetric lay-up in the present study, the in-plane shear residual stress approached zero, confirming the results of classical laminate theory for symmetric laminates (Ghasemi et al., 2014).

Tables 7 and 8 show that increasing the weight fraction of the CNTs combined with good dispersion can reduce the micro-residual stress in comparison with the nanocomposites having poor dispersion. As demonstrated in Tables 7 and 8, the micro-residual stress in the x- and y-direction decreased by 56.91 % and 37.65 %, respectively, in the well-dispersed nanocomposites with a 0.5 % CNT weight fraction in comparison with the composite without CNTs. In contrast to the poorly dispersed specimens, the higher weight fraction of CNTs increased the micro-residual stress. Tables 7 and 8 show that increasing the CNT weight fraction of poorly dispersed specimens caused the residual stress to increase 23.8% and 42.76%, respectively, compared to the composite without CNT in the x- and y-directions, respectively. This increase in residual stress is due to the stress concentration caused by CNT agglomeration. In fact, the CNT agglomerates act as particles in the structure of the matrix material and behave similarly to a non-homogenous substance. These materials do not behave predictably and generally have weaker characteristics than homogeneous materials.

As mentioned in section 5, the residual stress was calculated analytically using classical lamination theory to experimentally verify the value measured using the proposed method.

Due to the assumption of the modified Scharpery relation, only well-dispersed samples can be calculated and compared with the results of the experimental method. The CTE of the composites using different CNT weight fractions were obtained using Eqs. 9 and 10 as illustrated in Table 9. The results in Table 9 reveal that adding CNT to the matrix decreased the CTE of the laminate. As shown in the longitudinal and transverse directions, samples with higher CNT weight fractions showed a greater decrease in CTE.

After calculating the CTE of each layer, the resultant force and moments were determined using Eq. 12. The residual stress was calculated using Eq. 14 and the results are shown in Table 10 for composites without CNT and at two CNT weight fractions. In Eq. 12, ΔT was set as 90 °C from the experimental value used to fabricate the composite.

For each weight fraction of CNT, residual stresses of the composite obtained experimentally and analytically were compared and the differences are shown in Table 10 in the form of

Measurement direction	CNTs wt.%						
	0	0.1 % poor- dispersed	0.1 % well- dispersed	0.5 % poor- dispersed	0.5 % well- dispersed		
0°	60	55	45	68	30		
	[6.27]	[6.61]	[4.85]	[8.53]	[5.44]		
135°	-79	-61	-53	-98	-45		
	[5.34]	[7.21]	[7.95]	[9.14]	[6.31]		
270°	-330	-255	-190	-263	-139		
	[14.25]	[15.53]	[13.36]	[16.57]	[14.64]		

Table 6. Average value of experimentally measured strains (µɛ) in 0°, 135° and 270° gauge direction (standard deviation in brackets)

CNTs wt.%	0	0.1 % poor-dispersed		0.1% well-dispersed		0.5 % poor-dispersed		0.5% well-dispersed	
Layer No.	σ _{res} (MPa)	σ _{res} (MPa)	Δres%	σ _{res} (MPa)	Δres%	σ _{res} (MPa)	Δres%	σ _{res} (MPa)	$\Delta res\%$
1	-3.69	-2.94	-20.3	-2.59	-29.8	-4.46	20.87	-1.59	-56.91

Table 7. Residual stresses in x - direction in nanocomposites

CNTs wt.%	0	0.1 % poor-dispersed		0.1% well-dispersed		0.5 % poor-dispersed		0.5% well-dispersed	
Layer No.	σ _{res} (MPa)	σ _{res} (MPa)	Δres%	σ _{res} (MPa)	Δres%	σ _{res} (MPa)	Δres%	σ _{res} (MPa)	Δres%
1	3.24	2.72	-16.05	2.22	-31.48	4.12	27.16	2.02	-37.65

Table 8. Residual stresses in y - direction in nanocomposites

Thermal expansion coefficient μ /°C	CNTs wt.%					
	0	0.1 % well-dispersed	0.5 % well-dispersed			
Longitudinal Transverse	0.0837 29.3	0.0712 25.95	0.0544 19			

Table 9. CTE of each lamina

Residual stress MPa	Without CNT			0.1 % CNT			0.5 % CNT		
IVII a	Exp.	Theory	Error%	Exp.	Theory	Error%	Exp.	Theory	Error%
σ_{x} σ_{xy} σ_{y}	-3.69 -0.28 3.24	-3.42 0 3.42	7.9 - 5.3	-2.59 0.17 2.22	-2.51 0 2.51	3.2 - 11.5	-1.59 0.36 2.02	-1.76 0 1.76	9.6 - 14.8

Table 10. Comparison of residual stress obtained by experimental measurement and analytical method in well-dispersed nanocomposites

an error percentage. Good agreement can be observed between the experimental and analytical results for the composite without CNT and at the two CNT weight fractions. The maximum error percentage was observed in the composite with a 0.5 % CNT weight fraction at 14.8 %. The maximum shear stress measured experimentally was 0.36 MPa, which is negligible in comparison with the residual stress in other directions. The value of this shear stress coincided with the results of classical lamination theory at zero.

The arrangement used to fabricate the laminate nanocomposite was $[0_2/90_2]_s$ due to the symmetry of the arrangement. Using classical lamination theory, it was predicted that the tensile and compressive residual stresses would be equal along the thickness of the laminate composite. This is evident in Table 10.

According to classical lamination theory, the sum of all components of the residual stress $(\sigma_x, \sigma_y \text{ and } \sigma_{xy})$ must be equal to zero. The experimentally measured residual stress results are in good agreement with the theory.

7 Conclusions

The effect of CNTs on micro-residual stress was experimentally examined in the present study. Although a standard method of measuring residual stress exists at the macro-level, it is not applicable on a micro-scale because of the low accuracy of the strain gauges when measuring micro-strain. In order to measure the residual stress on a micro-scale, a laser beam was used to create a micro-hole of 180 µm in diameter. The SEM images were analyzed before and after formation of the micro-hole and the relieved strain was determined using the DIC method. To examine the accuracy of the present method, the residual macro-stress of the samples were first measured using a standard residual macro-stress measurement method and the results were compared with those from the present method. It has been demonstrated that the measured residual stress had acceptable accuracy.

It has been well-established that the addition of nanoparticles to polymer composites can generally improve their mechanical properties. The dispersion method for CNTs and the resulting agglomerates had an essential role in the performance of the nanocomposites. Two methods of dispersion were used in the present study and nanocomposites with slight and high agglomerations were fabricated.

To investigate the effects of CNT dispersion on the microresidual stress in the nanocomposites, the laser SEM-DIC method was employed and the released strain was experimentally measured. It has been shown that good dispersion reduced the micro-residual stress for the 0.1 % CNT weight fraction, but that CNT agglomeration increased the residual stress on a micro-scale for the 0.5 % CNT weight fraction. The FESEM images of CNT agglomerates show that a high stress concentration is the main reason for the increase in the micro-residual stress in the poorly dispersed specimens. Thus, the larger agglomerates increase the stress concentration and result in higher residual stress.

Therefore, the present experimental study reveals two important factors affecting micro-residual stress in nanocomposites: the dispersion quality and weight fraction of the CNTs.

Better dispersion quality and a higher weight fraction of CNTs will reduce the micro-residual stress.

Classical lamination theory as an analytical method were used to verify the residual stress results from the proposed experimental method. The assumptions of the modified Scharpery were used to calculate the CTE of the two-phase composites of a matrix and CNTs. The residual stress was calculated and compared in that of well-dispersed samples. Comparison of the analytical and experimental results showed acceptable accuracy with the proposed experimental measurements.

References

- Ahn, J., He, E., Chen, L., Pirling, T., Dear, J. P. and Davies, C. M., "Determination of Residual Stresses in Fibre Laser Welded AA2024-T3 T-Joints by Numerical Simulation and Neutron Diffraction", Mater. Sci. Eng.: A, 712, 685–703 (2018), DOI:10.1016/j.msea.2017.12.027
- Alamusi, Hu, N., Qiu, J., Li, Y., Chang, C., Atobe, S., Fukunaga, H., Liu, Y., Ning, H., Wu, L., Li, J., Yuan, W., Watanabe, T., Yan, C. and Zhang, Y., "Multi-Scale Numerical Simulations of Thermal Expansion Properties of CNT-Reinforced Nanocomposites", Nanoscale Res. Lett., 8, 15 (2013), DOI:10.1186/1556-276x-8-15
- Allain, S. Y. P., Gaudez, S., Geandier, G., Hell, J. C., Gouné, M., Danoix, F., Soler, M., Aoued, S. and Poulon-Quintin, A., "Internal Stresses and Carbon Enrichment in Austenite of Quenching and Partitioning Steels from High Energy X-Ray Diffraction Experiments", Mater. Sci. Eng., A, 710, 245–250 (2018), DOI:10.1016/j.msea.2017.10.105
- ASTM, D3039/D3039M-17: Standard Test Method for Tensile Properties of Polymer Matrix Composite Materials, ASTM International, West Conshohocken, PA (2017)
- ASTM, E837-13a: Standard Test Method for Determining Residual Stresses by the Hole-Drilling Strain-Gage Method, ASTM International, West Conshohocken, PA (2013)
- Baker, S., Matthews, I., "Lucas-Kanade 20 Years on: A Unifying Framework", Int. J. Comput. Vision, 56, 221–255 (2004), DOI:10.1023/B:VISI.0000011205.11775.fd
- Bert, C. W., Thompson, G. L., "A Method for Measuring Planar Residual Stresses in Rectangularly Orthotropic Materials", J. Compos. Mater., 2, 244–253 (1968), DOI:10.1177/002199836800200209
- Blaber, J., Adair, B. and Antoniou, A., "Ncorr: Open-Source 2D Digital Image Correlation Matlab Software", Exp. Mech., **55**, 1105–1122 (2015), DOI:10.1007/s11340-015-0009-1
- Ding, S., Wang, P., Lin, Y. and Zhu, D., "Reduction of Thermal Effect on Rail Stress Measurement Based on Magnetic Barkhausen Noise Anisotropy", Measurement, 125, 92–98 (2018), DOI:10.1016/j.measurement.2018.02.041
- Faghidian, S. A., "New Framework for Bayesian Statistical Analysis and Interpolation of Residual Stress Measurements", Mech. Res. Commun., 50, 17–21 (2013), DOI:10.1016/j.mechrescom.2013.02.008
- Faghidian, S. A., "A Smoothed Inverse Eigenstrain Method for Reconstruction of the Regularized Residual Fields", Int. J. Solids Struct., 51, 4427–4434 (2014), DOI:10.1016/j.ijsolstr.2014.09.012
- Faghidian, S. A., "A Note on the Inverse Reconstruction of Residual Fields in Surface Peened Plates", Lat. Am. J. Solids Struct., 12, 2351–2362 (2015a), DOI:10.1590/1679–78251811
- Faghidian, S. A., "Inverse Determination of the Regularized Residual Stress and Eigenstrain Fields due to Surface Peening", J. Strain Anal. Eng., 50, 84–91 (2015b), DOI:10.1177/0309324714558326
- Faghidian, S. A., "A Regularized Approach to Linear Regression of Fatigue Life Measurements", Int. J. Struct. Integrity, 7, 95-105 (2016), DOI:10.1108/IJSI-12-2014-0071

- Faghidian, S. A., "Analytical Approach for Inverse Reconstruction of Eigenstrains and Residual Stresses in Autofrettaged Spherical Pressure Vessels", J. Pressure Vessel Technol., 139, 041202-041202-7 (2017), DOI:10.1115/1.4035980
- Ghaedamini, R., Ghassemi, A. and Atrian, A., "Ring-Core Method in Determining the Amount of Non-Uniform Residual Stress in Laminated Composites: Experimental, Finite Element and Theoretical Evaluation", Arch. Appl. Mech., 88, 755–767 (2018), DOI:10.1007/s00419-017-1340-z
- Ghasemi, A. R., Mohammadi Fesharaki, M. and Mohandes, M. "Three-Phase Micromechanical Analysis of Residual Stresses in Reinforced Fiber by Carbon Nanotubes", J. Compos. Mater., 51, 1783–1794 (2017), DOI:10.1177/0021998316669854
- Ghasemi, A., Taheri-Behrooz, F. and Shokrieh, M. M., "Determination of Non-Uniform Residual Stresses in Laminated Composites Using Integral Hole Drilling Method: Experimental Evaluation", J. Compos. Mater., 48, 415–425 (2014), DOI:10.1177/0021998312473858
- Giri, A., Mahapatra, M. M., "On the Measurement of Sub–Surface Residual Stresses in SS 304L Welds by Dry Ring Core Technique", Measurement, 106, 152–160 (2017), DOI:10.1016/j.measurement.2017.04.043
- Hamidi, Y. K., Altan, M. C., "Process Induced Defects in Liquid Molding Processes of Composites", Int. Polym. Proc., 32, 527–544 (2017), DOI:10.3139/217.3444
- Hashin, Z., "Analysis of Properties of Fiber Composites with Anisotropic Constituents", J. Appl. Mech., 46, 543-550 (1979), DOI:10.1115/1.3424603
- Jain, M. K., Das, J., Deb, S., Subrahmanyam, J. and Ray, S., "Analysis of Residual Thermal Stresses in MoSi2 Based Laminated Composites", Int. J. Refract. Met. Hard Mater., 68, 9–18 (2017), DOI:10.1016/j.ijrmhm.2017.06.002
- Jana, M., Singh, R. N., "A Study of Evolution of Residual Stress in Single Crystal Silicon Electrode Using Raman Spectroscopy", Appl. Phys. Lett., 111, 063901 (2017), DOI:10.1063/1.4997768
- Jiang, W., Chen, W., Woo, W., Tu, S. T., Zhang, X. C. and Em, V., "Effects of Low-Temperature Transformation and Transformation-Induced Plasticity on Weld Residual Stresses: Numerical Study and Neutron Diffraction Measurement", Mater. Des., 147, 65-79 (2018), DOI:10.1016/j.matdes.2018.03.032
- Jimenez-Mena, N., Sapanathan, T., Drezet, J. M., Pirling, T., Jacques, P. J. and Simar, A., "Residual Stresses of Friction Melt Bonded Aluminum/Steel Joints Determined by Neutron Diffraction", J. Mater. Proc. Technol., 266, 651–661 (2019), DOI:10.1016/j.jmatprotec.2018.11.030
- Jones, K. W., Bush, R. W., "Investigation of Residual Stress Relaxation in Cold Expanded Holes by the Slitting Method", Eng. Fract. Mech., 179, 213–224 (2017), DOI:10.1016/j.engfracmech.2017.05.004
- Jones, R., Kinloch, A. J., Michopoulos, J. G., Brunner, A. J. and Phan, N., "Delamination Growth in Polymer-Matrix Fibre Composites and the Use of Fracture Mechanics Data for Material Characterisation and Life Prediction", Compos. Struct., 180, 316–333 (2017), DOI:10.1016/j.compstruct.2017.07.097
- Kollins, K., Przybyla, C. and Amer, M.S., "Residual Stress Measurements in Melt Infiltrated SiC/SiC Ceramic Matrix Composites Using Raman Spectroscopy", J. Eur. Ceram. Soc., 38, 2784–2791 (2018), DOI:10.1016/j.jeurceramsoc.2018.02.013
- Korsunsky, A. M., Salvati, E., Lunt, A. G. J., Sui, T., Mughal, M. Z., Daniel, R., Keckes, J., Bemporad, E. and Sebastiani, M., "Nanoscale Residual Stress Depth Profiling by Focused Ion Beam Milling and Eigenstrain Analysis", Mater. Des., 145, 55–64 (2018), DOI:10.1016/j.matdes.2018.02.044
- Lasaosa, A., Gurruchaga, K., Arizti, F. and Martínez-de-Guerenu, A., "Quantitative Estimation of Nonmonotonic Residual Stress Depth-Profiles Using an Extended Kypris–Jiles Model of the Magnetic Barkhausen Noise Spectrum", J. Appl. Phys., 123, 033904 (2018), DOI:10.1063/1.5002074

- Lin, J., Ma, N., Lei, Y. and Murakawa, H., "Measurement of Residual Stress in Arc Welded Lap Joints by Cos α X-Ray Diffraction Method", J. Mater. Proc. Technol., 243, 387–394 (2017), DOI:10.1016/j.jmatprotec.2016.12.021
- Nobre, J. P., Kornmeier, M. and Scholtes, B., "Plasticity Effects in the Hole-Drilling Residual Stress Measurement in Peened Surfaces", Exp. Mech., **58**, 369–380 (2018), DOI:10.1007/s11340-017-0352-5
- Pan, W. C., Tsai, A. T., Cheng, F. Y., Chen, T. Y. F. and Lin, M. T., "DIC Image on FIB Ring-Core Analysis of Depth Sensing Residual Stress Measurement of Thin Films", Advancement of Optical Methods & Digital Image Correlation in Experimental Mechanics, 3, 2019, DOI:10.1007/978-3-319-97481-1_15
- Pan, B., Asundi, A., Xie, H. and Gao, J., "Digital Image Correlation Using Iterative Least Squares and Pointwise Least Squares for Displacement Field and Strain Field Measurements", Opt. Lasers Eng., 47, 865–874 (2009), DOI:10.1016/j.optlaseng.2008.10.014
- Peral, D., de Vicente, J., Porro, J. A. and Ocaña, J. L., "Uncertainty Analysis for Non-Uniform Residual Stresses Determined by the Hole Drilling Strain Gauge Method", Measurement, 97, 51–63 (2017), DOI:10.1016/j.measurement.2016.11.010
- Salvati, E. and Korsunsky, A. M., "An Analysis of Macro- and Micro-Scale Residual Stresses of Type I, II and III Using FIB-DIC Micro-Ring-Core Milling and Crystal Plasticity FE Modelling", Int. J. Plasticity, 98, 123–138 (2017), DOI:10.1016/j.ijplas.2017.07.004
- Salvati, E., Benedetti, M., Sui, T., and Korsunsky, A. M., "Residual Stress Measurement on Shot Peened Samples Using FIB-DIC", Residual Stress, Thermomechanics & Infrared Imaging, Hybrid Techniques and Inverse Problems, 9, 275–283 (2016), DOI:10.13140/RG.2.1.4333.6800
- Schajer, G. S., Yang, L., "Residual-Stress Measurement in Orthotropic Materials Using the Hole-Drilling Method", Exp. Mech., 34, 324– 333 (1994), DOI:10.1007/BF02325147
- Schapery, R. A., "Thermal Expansion Coefficients of Composite Materials Based on Energy Principles", J. Compos. Mater., 2, 380–404 (1968), DOI:10.1177/002199836800200308
- Rahimian-Koloor, S. M., Moshrefzadeh-Sani, H., Shokrieh, M. M. and Hashemianzadeh, S. M., "On the Behavior of Isolated and Embedded Carbon Nano-Tubes in a Polymeric Matrix", Mater. Res. Exp., 5, 025019 (2018), DOI:10.1088/2053-1591/aaac4e
- Shah, P., Halls, V., Zheng, J. Q. and Batra, R. C., "Optimal Cure Cycle Parameters for Minimizing Residual Stresses in Fiber-Reinforced Polymer Composite Laminates", J. Compos. Mater., 52, 773–792 (2018), DOI:10.1177/0021998317714317
- Shokrieh, M. M., Daneshvar, A. and Akbari, S., "Reduction of Thermal Residual Stresses of Laminated Polymer Composites by Addition of Carbon Nanotubes", Mater. Des., 53, 209–216 (2014), DOI:10.1016/j.matdes.2013.07.007
- Shokrieh, M. M., Daneshvar, A. and Chitsazzadeh, M. "A Novel Method to Decrease Micro-residual Stresses of Fibrous Composites by Adding Carbon Nanotube", J. Ultrafine Grained Nanostruct. Mater., **46**, 61–66 (2013), DOI:10.7508/jufgnsm.2013.01.009
- Smit, T. C., Reid, R. G., "Residual Stress Measurement in Composite Laminates Using Incremental Hole-Drilling with Power Series", Exp. Mech., 58, 1221–1235 (2018), DOI:10.1007/s11340-018-0403-6
- SmithM2009 ABAQUS/Standard User's Manual Version 6.9. Simulia, Providence, RI (2016)
- Song, Y. S., Youn, J. R., "Influence of Dispersion States of Carbon Nanotubes on Physical Properties of Epoxy Nanocomposites", Carbon, 43, 1378–1385 (2005), DOI:10.1016/j.carbon.2005.01.007
- Xi, Y., Bai, Y., Gao, K., Pang, X., Yang, H., Yan, L. and Volinsky, A. A., "Residual Stress and Microstructure Effects on Mechanical, Tribological and Electrical Properties of TiN Coatings on 304 Stainless Steel", Ceram. Int., 44, 15851–15858 (2018), DOI:10.1016/j.ceramint.2018.05.266

- Xu, Y., Bao, R., "Residual Stress Determination in Friction Stir Butt Welded Joints Using a Digital Image Correlation-Aided Slitting Technique", Chin. J. Aeronaut., 30, 1258–1269 (2017), DOI:10.1016/j.cja.2016.11.003
- Zhang, Q., Xie, H., Liu, Z. and Dai, X., "Characterization of Micro-Scale Residual Stress around Thermal Grown Oxide Using Micro-Slotting Method and Geometric Phase Analysis", Meas. Sci. Technol., 29, 035202 (2018), DOI:10.1088/1361-6501/aa9f86
- Zhou, P., Jin, X., Chen, J., Zhou, Y., Luo, J., Li, H., Chu, C. and Yan, M., "Residual Stress Estimation in Laminated ZrB2-SiC Ultra-High Temperature Ceramics with Strong Interfaces Using X-Ray Diffraction and Indentation Techniques", Ceram. Int., 43, 12459–12465 (2017), DOI:10.1016/j.ceramint.2017.06.115
- Ziaei Moghadam, H. R., Faghidian, S. A. and Jamal-Omidi, M., "Agglomeration Effects of Carbon Nanotube on Residual Stresses in Polymer Nano Composite Using Experimental and Analytical Method", Mater. Res. Exp., 6, 035009 (2019), DOI:10.1088/2053-1591/aaf370

Date received: August 31, 2018 Date accepted: January 12, 2019

Bibliography DOI 10.3139/217.3756 Intern. Polymer Processing XXXIV (2019) 3; page 356–366 © Carl Hanser Verlag GmbH & Co. KG ISSN 0930-777X